Science of the Total Environment 782 (2021) 146932

Contents lists available at ScienceDirect

Science of the Total Environment

journal homepage: www.elsevier.com/locate/scitotenv

Remote sensing of inland Sabkha and a study of the salinity and temporal stability for sustainable development: A case study from the West coast of Qatar

Sankaran Rajendran [a,*], Hamad Al-Saad Al-Kuwari [a], Fadhil N. Sadooni [a], Sobhi Nasir [b], Himanshu Govil [c]

[a] Environmental Science Center, Qatar University, P.O. Box: 2713, Doha, Qatar
[b] Earth Sciences Department, Sultan Qaboos University, Al-Khod, 123 Muscat, Oman
[c] Department of Applied Geology, National Institute of Technology, Raipur, India

HIGHLIGHTS

- Remote sensing of inland sabkha of Qatar is studied for sustainable development.
- Minerals and rock types of sabkha are mapped using Hyperion and ASTER data.
- Salinity of sabkha region is monitored using Sentinel-2 data by NDSI index.
- Applications of satellite data are validated by field and laboratory studies.
- Capability of sensors is demonstrated to study the sabkha of arid region.

GRAPHICAL ABSTRACT

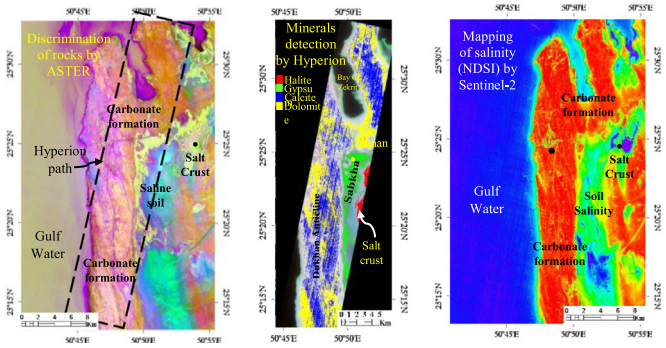

ARTICLE INFO

Article history:
Received 24 January 2021
Received in revised form 27 March 2021
Accepted 30 March 2021
Available online 6 April 2021

Editor: Fernando A.L. Pacheco

Keywords:
Remote sensing
Inland Sabkha
Salinity
Temporal stability
Dukhan
Qatar

ABSTRACT

The inland sabkha of the Arabian Gulf is important to study for the occurrence of minerals, rocks, soil salinity, and stability of the sabkha due to the high demand for infrastructure and agriculture development region. This study describes the spectral absorptions of evaporite minerals, discriminates rocks, maps salt crusts, gypsiferous soil flats, and soil salinity, and studies the temporal stability of an inland sabkha of the Dukhan area, west coast of the State of Qatar. This was performed using satellite data of the Hyperion of EO1, ASTER of Terra, and multispectral instrument (MSI) of Sentinel-2. The occurrence of minerals in the area is detected using Hyperion data by the linear spectral unmixing (LSU) method and studied for their spatial distribution. The different geological formations of the sabkha were discriminated by using the VNIR (visible and near-infrared) and SWIR (shortwave infrared) spectral bands from ASTER by principal component analysis (PCA). The image developed by using the principal components (R:PC2, G:PC3, B:PC5) showed the formations in different tones. Salinity of the area was mapped using monthly data of MSI from 2018 to 2020 by normalized difference salinity index (NDSI) (band11-band12)/(band11 + band12). The results of the index displayed the distribution of salinity in the area. Besides, moisture of the area was studied by using the normalized difference moisture index (NDMI) (b8-b11)/(b8 + b11) and described the temporal stability of the sabkha. All the results of image analyses were validated through field and laboratory studies. The study of laboratory spectra of evaporite minerals namely gypsum, anhydrite, and halite present in the salt crusts and gypsiferous soil flats showed their unique spectral absorptions in between 1.4–1.5 μm and 1.9–2.0 μm whereas, the calcite and dolomite minerals of the carbonate formations exhibited deep absorptions near 2.345 and 2.495 μm respectively.

* Corresponding author.
E-mail address: srajendran@qu.edu.qa (S. Rajendran).

https://doi.org/10.1016/j.scitotenv.2021.146932

1. Introduction

Sabkha (an Arabic word meaning salt flat) of arid, semi-arid, and sub-humid regions has aggressive environments. The soils of sabkha consist of concentrated brine where the salts are a serious problem to the development and sustainable utilization of land resources in the region (Saeed et al., 2020; Al-Homidy et al., 2017; Basyoni and Aref, 2016). Factors affecting the development of evaporite minerals and sabkha in the region include climate, geomorphology, and chemical composition (Censi et al., 2020; Chenchouni, 2017; Schulz et al., 2015). Fluctuations in temperature and humidity in the region form various salts of chloride and sulfate in the capillary "vadose" zones (Alharbi et al., 2012; Bai et al., 2011; Rongjiang and Jingsong, 2010) and the quality of soils of the sabkha mainly depends on the presence of the amount and types of salts such as anhydrite ($CaSO_4$), calcite ($CaCO_3$), gypsum ($CaSO_4.2H_2O$), Halite (NaCl), and dolomite ($CaMg(CO_3)_2$) (Censi et al., 2020). Thus, naturally existing soils of the sabkha often have loose, low density, unstable, and low compression strength characters (Al-Amoudi and Abduljauwad, 1995) and are unacceptable for the use of normal practices (Al-Amoudi, 1994). Sabkha of the arid Arabian region extends intermittently with different extensions along the Gulf coasts (Fig. 1). The study of the concentration of salts in the coastal sabkha of the Arabian Gulf by Dhowian et al. (1987) showed the presence of higher salts which is 4 to 5 times higher than the Gulf water. The understanding of changes in the brine composition due to periodic wet-dry cycles and the development of evaporite minerals of this region requires multitemporal observations to assess the stability of sabkha (Lokier, 2013). Thus, mapping of salinity and the temporal stability of sabkha in the arid is important especially, in the State of Qatar where the sabkhas areas are considered for infrastructural and agricultural development due to the dramatic rise in the population, industry, and agriculture (Khalil et al., 2020). However, the limited accessibility of sabkha environments makes it difficult to study by field mapping.

In this connection, remote sensing techniques have the potential to detect evaporite minerals, discriminate sabkha, and map salt crust and saline soils. The techniques are capable of monitoring sabkha regions and provide details for their spatial distribution to assess their suitability for development (Bannari and Al-Ali, 2020; Gorji et al., 2019; Abuelgasim and Ammad, 2019). A literature review shows that the VNIR parts of the electromagnetic spectrum are sensitive to detect salt crust and salt flats of sabkhas and the spectral regions can be used to map saline soils (Gorji et al., 2019; Bannari et al., 2018, 2016; El-Battay et al., 2017). The studies, based on the hyperspectral imagery, show better identification and quantification of evaporite minerals (Abd El-Hamid and Hong, 2020; Milewski et al., 2017; Riaza et al., 2017). Field exposure of salts can be well identified by using the multispectral satellite data due to the high reflectance of salts that depend on characters such as color, mineralogy, surface smoothness, and type of salts (Bannari et al., 2018, 2016; Al-Hemoud et al., 2020; Dematte et al., 2004; Mougenot et al., 1994). Especially, the data that have high spectral and spatial resolutions provide the best results and allow us to develop different salinity indices to detect the salt-affected areas (Elhag, 2016; Allbed et al., 2014). Indices developed using spectral bands that characteristics to spectral absorption of saline soils have the potential to show the occurrence of salt crusts (Nguyen et al., 2020; Guo et al., 2019; Gorji et al., 2019).

Although several studies were carried out to map salt-affected areas and model soil salinity of sabkha regions using remote sensing technique (Abuelgasim and Ammad, 2019; Khawfany et al., 2017), the study to assess the occurrence and distribution of salt crusts, salt flats, and saline soil of an inland sabkha of the arid region using remote sensing is limited. Therefore, this study aims to map the dynamic change in the spatially and temporally distributed salt crust and saline soil flats of an inland sabkha that occurred near Dukhan in the northwest coastal region of Qatar (Fig. 1). The major objectives are 1) to describe the spectral band absorptions of evaporites and map the minerals of the sabkha using Hyperion data of EO-1, 2) to discriminate the salt crust, gypsiferous sand and silt flats, and carbonate formations of the area using ASTER (Advanced Spaceborne Thermal Emission and Reflection Radiometer) data of Terra, and 3) to characterize the soil salinity and moisture of the area using MSI data from Sentinel-2 to understand the occurrence and spatial distribution of the evaporites, salt crusts, salt flats of the area and temporal stability of the sabkha in an arid climate. This study evaluates remote sensing results by conducting fieldwork and analyzing field samples in the laboratory. The study of soil salinity and temporal stability of sabkha using remote sensing techniques is important to scientists and environmentalists and useful to governmental decision leaders, planners, and investors to plan and develop infrastructure and agriculture in the sabkha areas.

2. Dukhan Sabkha

The sabkha area studied is located near Dukhan on the west coast of the State of Qatar (Fig. 1). It occupies an area of 73 km^2 and is the largest inland sabkha in the Arabian Gulf. The sabkha has a length of approximately 20 km and a width of 2 to 4 km (Howell et al., 2010). This area of sabkha is characteristic of little annual rain events between October and May and completely dry from June to September (Cheng et al., 2017). A previous study reports that the parts of sabkha in the north lie below sea level and receive some seawater from Zekreet Bay which is situated at a distance of approximately 3 km to the north (Ajmal Khan et al., 2006; Al-Thani, 1992). Also, geologists have put forward that the sabkha could have been an extension of the bay approximately 3000 years ago (Ashour, 2013). The Rawdat Jarrah depression is situated between the bay and the sabkha (Fig. 1).

Study of the stratigraphy and paleogeography of Qatar shows that the geological formations of Qatar are part of the Arabian Gulf sedimentary basin dominated by formations from the Tertiary and Quaternary ages. There are three major formations namely 1) the Umm er Radhuma Formation (Paleocene-Lower Eocene), (2) the Rus Formation (Lower Eocene), and (3) the Dammam Formation (Middle Eocene), and the formations are dissected by high-angle faults (Al-Saad, 2005; Cavelier et al., 1970; Rivers et al., 2019; Rivers and Larson, 2018). Among the formations, the Umm er Radhuma Formation and the lower part of the Rus formation do not crop out, while the upper part of the Rus and Dammam formations are well exposed on the surface (Al-Saad and Hewaidy, 2020; Boukhary et al., 2011; Fig. 1c). Recently, Rivers et al. (2019) stated that the Umm er Radhuma Formation and the overlying Rus Formation (Traina Member) were deposited in two different marine basins. They described that the southern basin was deposited by extensive evaporites and clay-rich siliciclastics during the early periods of the Rus Formation and the deposits were not observed in the comparable strata of northern basin. The northern basin was deposited by fossiliferous limestone and ferruginous chalky limestone of Rus formation (Al Khor Member) and the Dammam Formation. The Dammam Formation consists of five members namely the Rujm Aid, Midra Shale, Umm Bab, Alveolina, and the Abaruq Members, and exposed well in the northern part of Qatar (Al-Saad, 2005; Cavalier, 1975; Cavelier et al., 1970). They stated that the deposits of Al Khor Member and Dammam Formation of the basins were interconnected. The Dammam Formations are overlined by the Dam Formation of Middle Miocene age and Hofuf formation of Miocene and Pliocene ages. These formations were deposited over by the miliolite of the Pleistocene age and the coastal and aeolian deposits of the Quaternary age. The large areas of sabkha of Quaternary age occurred mostly on the east coast and the inland sabkhas have occurred near the east of Dukhan.

Fig. 1 shows the occurrence of Rus and Dammam Formations and the distribution of sabkha and aeolian deposits in the study area. The Rus Formation (Er) consists mainly of dolomitic and chalky limestone (Al-Saad and Hewaidy, 2020; Al-Hajari and Kendall, 1992). The Dammam Formation occurs as a sequence of hillocks consisting of limestone and dolomite (Edm1, Edm2AM, and Edm2SM) (Fig. 1a; Nasir et al., 2008;

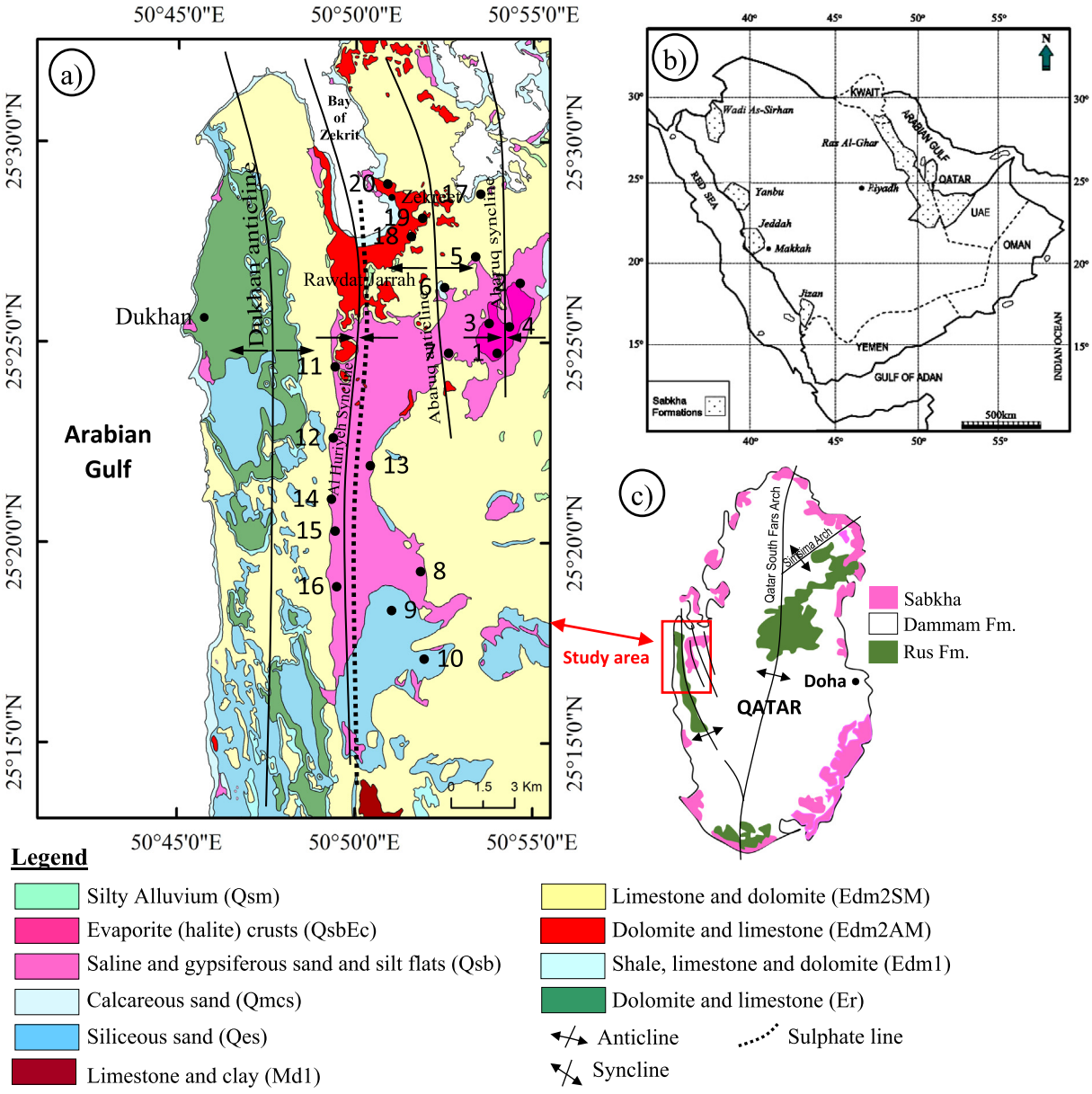

Fig. 1. Showing a) the geology of Dukhan region, State of Qatar (Al-Saad and Hewaidy, 2020; Geological map of Qatar, 2007; Al-Youssef et al., 2006. The dotted sulfate line is from Dill et al. (2005). Locations represent the soil samples collection); b) the distribution of sabkha soils in the Arabian Peninsula (Al-Amoudi et al., 1992); c) the distribution of sabkha, and Rus and Dammam Formations in the State of Qatar (Al-Saad and Hewaidy, 2020).

Al-Saad, 2005). The Dam formation consists of fossiliferous limestone, marl, and clay (lagoonal and marine deposits) that occur in the south of the study area. The formation is deposited over by the siliceous sands and silts (Qes) and marine calcareous sands (Qmcs) of the Quaternary age. Sabkha in the study area is characterized by the presence of evaporite (halite) crust (QsbEc) and gypsiferous sand and silt flats (Qsb) (Al-Youssef et al., 2006). Dill et al. (2005) interpreted a line of sulfate occurrence over the gypsiferous sand and silt deposits. There are numerous aeolian dunes in the study area. The area has alternating anticlines (Dukhan and Abaruq anticlines) and synclines (Al Huriyeh and Abaruq synclines), and a group of fold structures that run parallel to the west coast in an NNW to SSE direction (Fig. 1; Leblanc, 2008). The Dukhan anticline has a length of about 80 km and stands out from the neighboring folds with steep dips. Folding is more pronounced in the north of the study area and the structure is associated with deep-seated salt movements (Leblanc, 2015; Dill et al., 2003).

3. Data and methodology

3.1. Satellite data

This study mapped evaporite minerals, salt crusts, salt flats, soil salinity, and other geological formations in the study area using data from Hyperion of EO1, ASTER of Terra, and MSI of Sentinel-2 satellites (Table 1 in Appendix-A). The detection of minerals was carried out using the Hyperion data by Linear Spectral Unmixing (LSU) method (Singh, 2018; Rajendran and Nasir, 2017). The geological formations of the area are discriminated by the processing of the visible and near-infrared and shortwave infrared bands of ASTER by principal component analysis (PCA) (Rajendran and Nasir, 2019; Ge et al., 2018; Kumar et al., 2015). Soil salinity of the area and the temporal stability of sabkha were studied by analyzing the spectral bands of MSI using Sentinel-2 indices such as the Normalized Difference Salinity Index

(NDSI) and the Normalized Difference Moisture Index (NDMI). Hyperion and ASTER data were obtained from the USGS Data Management and Information Distribution (DMID) (https://glovis.usgs.gov/) and MSI data were collected from European Space Agency (ESA) at the Copernicus Open Access Hub. The sensor characters are given in Table 2 in Appendix-A.

3.1.1. Pre-processing of data

i. Hyperion data

Hyperion of EO-1 satellite provides 242 spectral bands at a bandwidth of ~10 nm in the spectral region of 400–2500 nm. The sensor covers a spatial extent of 7.5 km width and 105 km length, and a spatial resolution of 30 m (Pearlman et al., 2003; Table 2 in Appendix-A). The signal-to-noise ratio (SNR) of the VNIR detector is from ~140:1 to 190:1 and for the SWIR detector is from 96:1 to 38:1 (Pearlman et al., 2003). The data, acquired on March 5, 2010, was preprocessed and minerals of the study area were mapped (Table 1 in Appendix-A). The preprocessing of data included rescaling of radiance, removal of spectrally overlapping bands, bad bands, de-striping, smile effect correction, geometric rectification, and atmospheric correction (Goodenough et al., 2003) and was carried out using ENVI image processing software (ENVI 5.5, Harris Geospatial Solutions, CO, USA; https://www.harrisgeospatial.com). During which, bands that had no spectral information (bad and un-calibrated bands such as 1–9, 58–81, 120–128, 165–174, and 225–242) were removed and a total of 168 bands (45 in VNIR and 123 in SWIR) were used in this study. The Hyperion Level 1R product was not geometrically corrected and therefore the data were georeferenced using Ground Control Point (GCP) selection (a total of 15 points) and first-order transformation with an overall root-mean-square error (RMSE) of 0.001720. The scattering of molecular and particulates, absorption at the radiance-at-sensor, and retrieve of the values of reflectance-at-surface was carried out using the Fast Line-of-site Atmospheric Analysis of Spectral Hypercubes (FLAASH) tool (Perkins et al., 2012; Anderson et al., 2002).

ii. ASTER data

ASTER has three bands in the VNIR, six in the SWIR, and five bands in the TIR wavelength regions and the bands have 15 m, 30 m, and 90 m spatial resolutions, respectively (Table 2 in Appendix-A; Fujisada, 1995). To map the geological formations of the study area (Fig. 1), two cloud-free Level 1 ASTER data from July 22, 2003, were obtained (Table 1 in Appendix-A) and used. The data have less than 2% cloud cover and the registration of imageries was carried out using the GCPs. Radiometric, geometric and atmospheric corrections were applied to the data and carried out using FLAASH after a correction for cross-track illumination to remove the water vapor and aerosols effects found on the data.

iii. MSI data

MSI data of Sentinel-2 has 13 bands in the VNIR to SWIR spectral region with spatial resolutions of 10 m, 20 m, and 60 m to study the spatial information of earth surface features (Table 2 in Appendix-A; ESA, 2015). In this study, we collected MSI Level-1C monthly data of the years from 2018 to 2020 (Table 1 in Appendix-A) and used them to study soil salinity of the area. The data were preprocessed using the Sentinel Application Platform (SNAP) program which has the Sen2Cor plugin and Sentinel-2 Toolbox (http://step.esa.int/main/toolboxes/snap/) (Louis et al., 2016; Clevers and Gitelson, 2013). Bands 1, 9, and 10 dedicated for coastal aerosol, water vapor, and cirrus studies respectively were not included during the processing.

3.2. Image processing

3.2.1. Mapping of minerals

Several studies show mapping of minerals using Hyperion data by spectral analysis (Abd El-Hamid and Hong, 2020; Abubakar et al., 2019; Govil et al., 2018). In this study, the minerals of the gypsiferous sand and silt flats, salt crusts, and carbonate formations of the study area were carried out using the Hyperion data by linear spectral unmixing (LSU) method (Singh, 2018; Rajendran and Nasir, 2017). To detect the minerals, the endmembers that were collected from the edges of the data cluster were used, since the spectra collected from the field were not acquired under the same conditions of the data, and the endmembers are directly correlated with the features detectable in the data. But, the study of the absorption characters of minerals using the USGS Spectral Library and the spectra collected over the field samples were considered for using such endmembers in this study. The LSU method has been proven for mapping evaporite minerals, rock types, salt crusts, and salt-affected soils (Milewski et al., 2017; Zhang et al., 2014).

3.2.2. Discrimination of rock types

Several studies have been carried out mapping the rock types of arid regions using ASTER data (Rajendran and Nasir, 2019; El-Janati et al., 2014; Mars and Rowan, 2010). In the present study, mapping of Rus and Dammam Formation, siliceous sand deposits, gypsiferous sand, and silt flats and salt crust of the study area were carried out using the VNIR-SWIR bands by PCA method by studying the eigenvectors of the bands. The PCA method has been widely used to discriminate rock types, mineralized zones, and alterations of arid regions (Rajendran and Nasir, 2019, 2015; Ge et al., 2018; Kumar et al., 2015).

3.2.3. Study of soil salinity and temporal stability

Remote sensing of the salinity of soils portrays higher values in the SWIR region and relatively lower values in the NIR region (El-Battay et al., 2017; Nawar et al., 2014). Studies of soil salinity in arid regions using Sentinel-2 were carried out by Wang et al. (2019), Taghadosi et al. (2019), and Bannari et al. (2018). In this study, soil salinity of the sabkha region was studied using the MSI data from 2018 to 2020 and a salinity index of NDSI (band11-band12)/(band11 + band12) that provided in the Index database (IDB) for Sentinel-2 remote sensing indices (https://custom-scripts.sentinel-hub.com/custom-scripts/sentinel-2/indexdb/). The index was originally derived from ASTER bands (B4-B5)/(B4 + B5) by Al-Khaier (2003) to map the salinity of soils of the Balikh basin located in the northern part of Syria. Besides, this study uses the Normalized Difference Moisture Index (NDMI) (b8-b11)/(b8 + b11) and analyzes the moisture of the study area to understand the temporal stability of the Dukhan Sabkha.

3.3. Field and laboratory studies

Field studies were carried out in the study area between 2019 and 2020 to verify the results of satellite images and validate the occurrence of minerals, rock types, salt crusts, and saline soils of the salt flats. During the studies, the occurrence of evaporite minerals, carbonate rocks, and saline soils were verified. Further, field photographs were taken and samples were collected over the homogeneous top surface using a GPS for laboratory studies. The samples were used to measure reflectance spectra using a PIMA spectrometer to understand the spectral absorptions of the minerals and rocks of the area and map them over satellite data (Rajendran and Nasir, 2017, 2015). Samples from field studies were further used for mineral identification using an X-ray Diffractometer (MiniFlex II, Rigaku, Japan) and the mineral phase identification software (PDXL 2 Version 2.6.1 from Rigaku) to confirm the presence of minerals in the area. Also, soil and mineral samples of the area were measured for salinity, electrical conductivity (Ec), total dissolved solids (TDS), and potential of hydrogen (pH) using the

instruments YSI pH 100 and YSI EC 300 in the laboratory to understand the salinity of the sabkha and confirm the results of NDSI.

4. Results and discussion

4.1. Spectral absorptions of evaporites

Remote sensing of saline crusts that have bare soils of different types show significant shortwave infrared (SWIR) spectral absorption (Elnaggar and Noller, 2009; Metternicht and Fermont, 1998). However, mapping of evaporite minerals, salt crusts, and salt flats requires a complete understanding of the absorptions of such minerals and a proper selection of spectral bands (Drake, 1995). Nawar et al. (2014) studied the spectral absorption features of salt-affected soils and showed the presence of two deep absorptions at 1415 and 1915 nm, and weak absorption features around 1748, 2207, and 2385 nm. Bannari et al. (2018) measured the spectra of soil samples that have extreme saline (Sabkha) and non-saline (agricultural fields) using a high-resolution spectroradiometer and showed the presence of the absorption features of gypsum at 1000, 1210, 1450, 1490, 1540, 1748, 1780, 1945, 1975, 2175, 2215, 2265, and 2496 nm. They described the presence of strong absorption features for water at 975, 1190, 1450, and 1945 nm.

In this study, the laboratory spectra of evaporite minerals such as anhydrite ($CaSO_4$), gypsum ($CaSO_4.2H_2O$) and halite ($NaCl.2H_2O$), and the carbonate minerals namely calcite $CaCO_3$ and dolomite $CaMg(CO_3)_2$ were studied for their spectral absorptions to map the minerals and rocks that present in the area. Fig. 2a shows the spectra of minerals stacked from the USGS spectral library in the 0.5–2.5 μm wavelength. The plot shows the absorption features of gypsum between 0.97 μm and 2.5 μm in the SWIR region. The gypsum exhibits deep absorptions in between 1.4–1.5 μm and 1.9–2.0 μm (solid vertical lines) due to the presence of H_2O in its contents (Cloutis et al., 2006; Crowley, 1991; Clark et al., 1990). The halite and anhydrite show very weak absorptions between 1.4 μm and 1.5 μm and weak absorptions between 1.9 μm and 2.0 μm when studied with the spectra of gypsum. Several authors reported that the halite has absorptions near 1.4, 1.9, and 2.25 μm (Bannari et al., 2018; Farifteh et al., 2008). The dolomite and calcite minerals exhibit deep absorptions around 2.345 μm and 2.495 μm (dashed vertical lines) respectively, due to the presence of CO_3 in its contents (Fig. 2a; Clark, 1999; Van der Meer, 1995; Gaffey, 1987).

We also measured the spectra of halite (salt crust), gypsum, and anhydrite (of salt flats) minerals of the Dukhan sabkha and the carbonate rocks of Dammam and Rus Formations in the 1350 to 2500 nm range in the laboratory (Fig. 2b and c). Study of the spectra of gypsums (Gyp2, 5, 12, and 15) showed the presence of a broad triplet absorption between 1450 and 1550 nm and deep and broad absorptions around 1750 nm and in between 1900 and 2000 nm (solid vertical lines, Fig. 2b). The absorptions in the wavelengths are due to the presence of H_2O contents in the minerals. The anhydrite (Any3 and Any7) and halite (Hal6) exhibit strong absorptions between 1400 and 1500 nm and deep absorptions between 1900 and 2000 nm (dashed vertical lines) (Singh et al., 2018; Bishop et al., 2014). Halite is more reflective and exhibits a week absorptions around 1400 and 1900 nm when compared to the spectra of other minerals. Dolomite samples of the Rus formation (Dol5, 16, and 21) display absorptions near 1915, 1920, and 2330 nm (dashed vertical lines), and the limestone samples of the Dammam formation (Lst3, 7, 9, and 12; Fig. 2c) show absorption near 1420, 1930, 1995, 2160, 2220, and 2343 nm (solid vertical lines). The deep absorption at 2343 nm in the limestones and 2330 nm in the dolomite are characteristic of the presence of carbonates in the samples (Rajendran and Nasir, 2017).

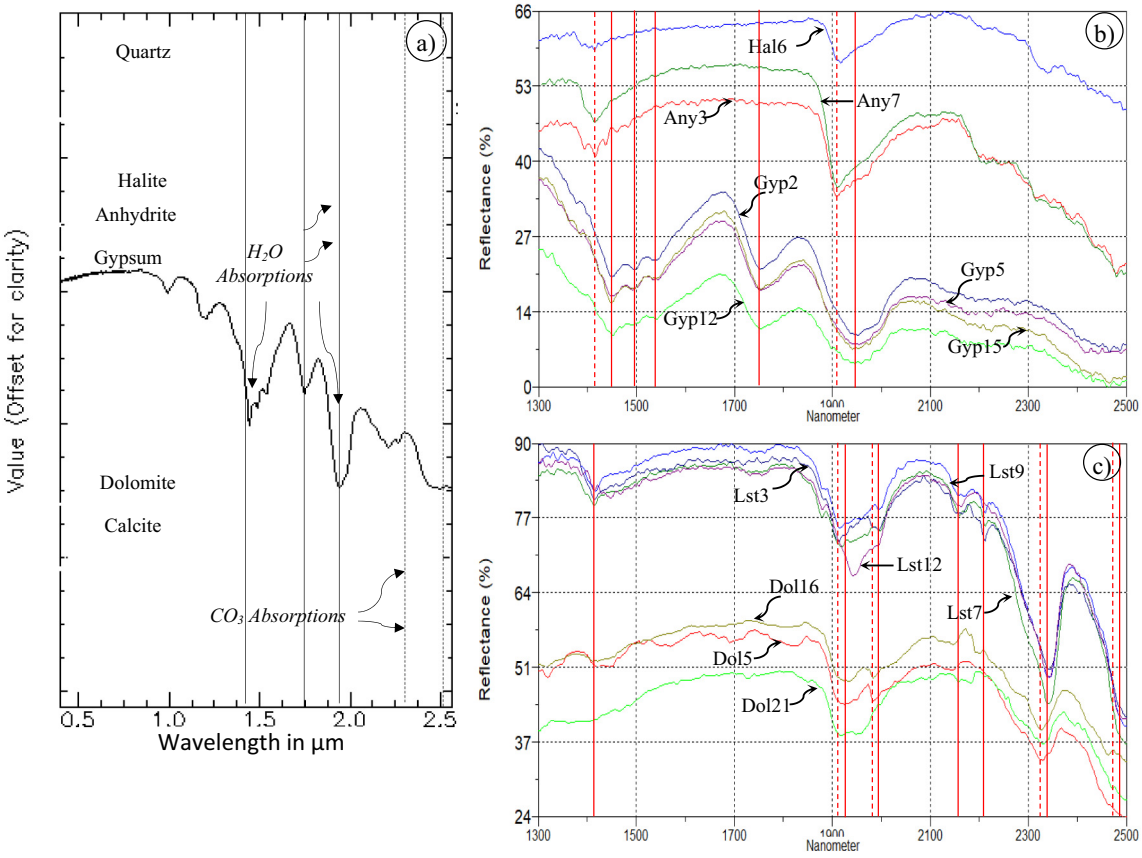

Fig. 2. Spectral plots stacked from a) the USGS Spectral Library for minerals; b) the PIMA spectra of gypsum, anhydrite, and halite minerals of the Dukhan sabkha; c) the dolomite minerals in the dolomite of Rus Formation and calcite minerals in the limestone of Dammam Formation of the study area.

Interpretations of the spectra of samples reveal that the minerals of the sabkha region have unique absorptions in the SWIR bands and the bands of ASTER in the wavelengths can be used to map the evaporites, salt crusts, saline soils, and carbonate rocks of the region.

4.2. Minerals mapping of Hyperion

4.2.1. Hyperion spectral absorptions

We studied the contiguous hyperspectral bands of Hyperion data (Fig. 3a) for spectral absorptions of the minerals. The image spectra collected based on field knowledge (Fig. 1 in Appendix-B) over the pixels of gypsiferous soil flats (HySp5 and HySp6), halite salt crusts (HySp7 and HySp8), and carbonate rocks of the Dammam formation (HySp1 and HySp2) and Rus formation (HySp3 and HySp4) are stacked and given in Fig. 3a. The spectral plot shows the presence of prominent absorptions in the gypsum and halite minerals that occurred in the gypsiferous soils and salt crusts. The spectra of minerals exhibit broad absorptions between 1400 and 1500 nm (red elliptical) and deep absorptions near 1750 nm (dashed red elliptical) which are comparable to the spectral absorptions of 1450–1550 nm and 1750 nm measured over the gypsum and halite samples collected from the field (see Fig. 2b). As well, the Hyperion spectra of carbonate minerals (Fig. 3a) exhibit narrow and deep absorptions at 1400 nm (blue elliptical), and deep and broad absorptions between 2200 and 2350 nm (blue dashed elliptical) which can also be compared with the spectra measured over the carbonate rock samples (see Fig. 2c). The spectral absorptions in the evaporites of the sabkha region are owing to the presence of water in the evaporite minerals (Warren, 2006). The absorptions between the 2200 and 2350 nm in the carbonate minerals are a result of the presence of carbonates in the limestone and dolomite formations (Aljerf, 2016). The spectra collected over the gypsiferous soil surface (HySp5 and HySp6) showed the presence of strong absorptions near 1750 nm and 2200–2350 nm when compared with the spectra of halite salt crusts (Hysp7 and 8) which may be due to the mixing of the minerals in the soil.

4.2.2. Minerals mapping

To understand the occurrence and distribution of minerals in the study area, we chose the image endmembers of Hyperion imagery that represent the minerals of the salt crusts, gypsiferous flats, carbonate rocks, and mapped the minerals by the LSU method. The result of the mapping is given in Fig. 3b. The image shows the occurrence of minerals and their relative distributions over the salt crusts, gypsiferous salt flats, and the carbonate formations of the area. The halite minerals (red) are found and distributed over the salt crust and the gypsums (green) are observed over the saline and gypsiferous sand and silt flats. The image exhibits the presence of calcites (blue) and dolomites (yellow) minerals over the dolomite and limestone rocks of the Rus and Dammam Formations respectively. The distribution of minerals can be studied with geology (Fig. 1).

4.3. Lithological discrimination of ASTER

The PCA matrix (Table 3 in Appendix-A) was used to identify the PC that contains information about the presence of the evaporite crusts, gypsiferous sand and silt flats, and carbonate formations of the area. The matrix provided the eigenvalues in the order of 98.18, 1.61, 0.10, 0.04, and 0.02 percentages for the first five PCs among the components. The PC1 scored the highest positive value in band 1 when compared to the other components and the image of the component exhibited the evaporite crust in grey and the other formations in white (Fig. 2a in Appendix-B). The PC2 provided the highest positive value in band 2 and the image showed the gypsiferous sand and silt flats in dark and the carbonate formations in white (Fig. 2b in Appendix-B). The Dammam Formation can be distinguished in very bright on the image. The image of PC3 (Fig. 2c in Appendix-B) showed the evaporites in bright and

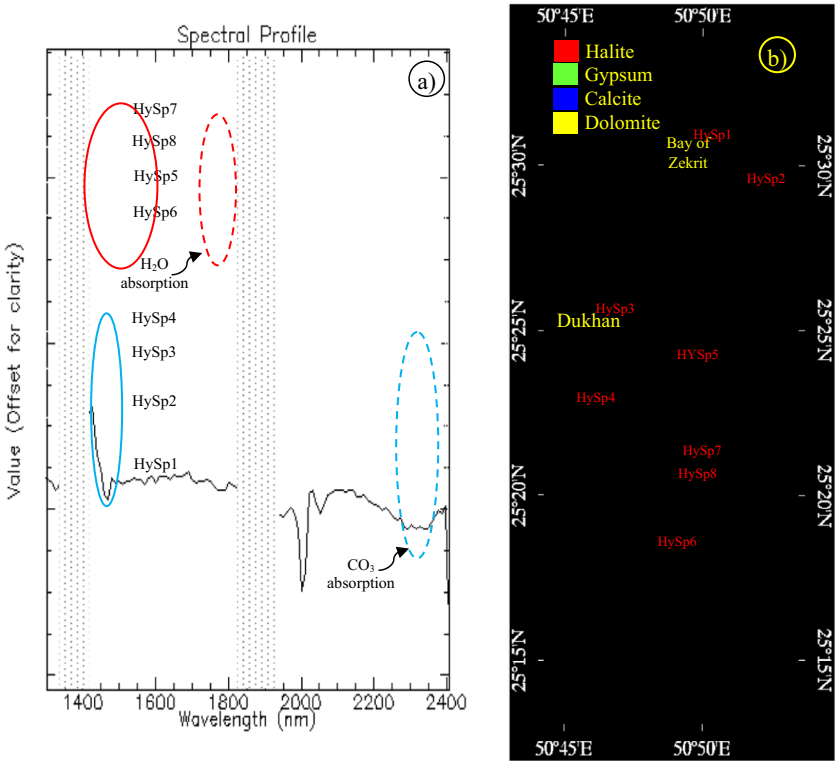

Fig. 3. Showing a) the spectral plot (1300 to 2400 nm wavelength) of minerals of the gypsiferous soil flat (Hysp5 and Hysp6) and halite salt crust (Hysp7 and Hysp8) of sabkha (Red ellipticals) and carbonate minerals of the Dammam (Hysp1 and Hysp2) and Rus (Hysp3 and Hysp4) Formations, the water absorption bands are masked by dotted lines; b) Hyperion image showing the occurrence and distribution of minerals of the salt crust, gypsiferous flat and Rus and Dammam Formations in parts of the study area.

carbonate formations in grey and provided the highest value in band 3 (Table 3 in Appendix-A). The PC4 provided the maximum value in band 5 and the component image (Fig. 2d in Appendix-B) did not show any formation of the study area distinctly. Whereas, the eigenvalue of PC5 provided the highest positive values in bands 4 and 6 and a negative value in band 5, and the PC image (Fig. 2e in Appendix-B) showed the Rus Formation in bright and the calcareous sand deposit in the dark. The components PC6 to PC9 provided values less than 0.1% (Table 3 in Appendix-A) and the images of components exhibited more noises.

Since the PC2, PC3, and PC5 provide useful information for the occurrence of different formations of the area, an image was produced using the components (R:PC2, G:PC3, B:PC5) to discriminate the evaporite crusts, salt flats, and other formations of the study area. The resulted image is given in Fig. 4. It exhibits all the formations in different tones and easily distinguishable except the minor occurrences of the silty alluvium and the limestone and clay deposits due to the spatial resolution of data. The image exhibits the Rus Formation (Er) in magenta, Dammam Formation (Edm2AM and Edm2SM) in yellowish-brown, and the calcareous sand (Qcms) in dark brown with fine to medium textures (Fig. 4). The siliceous sand deposits (Qes) that occurred over the carbonate formations appear in very light pink. The deposits that occurred inland exhibit greenish cyan with fine to medium textures which may be due to the presence of sulfates in the deposits. The gypsiferous sand and silt flats (Qsb) show yellow and the evaporite crust (QsbEc) exhibits shades of light yellowish pink with fine texture. The occurrence of siliceous sand and silts over the salt flats shows the shades of blue with fine texture. The discrimination of the salt crust, the gypsiferous salt flats, and carbonate formations can be studied with the geology map of the area (Fig. 1).

4.4. Soil salinity and temporal stability of sabkha

4.4.1. Soil salinity of Dukhan sabkha

Taghadosi et al. (2019) retrieved the soil salinity of Kuh Sefid village in the Qom Province, Iran using the Sentinel-2 and Landsat 8 data, and salinity indices. They stated that the indices can be considered for monitoring the soil salinity and mapping of EC of the soil of the area. Also, Bannari et al. (2018) described the sensitivity of VNIR-SWIR bands of MSI to discriminate the soil salinity of Bahrain. They demonstrated the capability of SWIR bands and the limitation of VNIR bands for the discrimination of salinity. They stated that the SWIR bands are an excellent candidate for monitoring and modeling the soil salinity at different scales. In this study, the monthly data of Sentinel-2 were analyzed for the years 2018 to 2020 using NDSI and the results are provided in Fig. 5 by assigning a rainbow color (represents the lowest value in violet and the highest value by red). The images of NDSI show the area of soil salinity (SSA) in green bounded by yellow with fine texture in the area of gypsiferous sand and silt flats (Figs. 1 and 5). The salinity is low over the siliceous sand deposits and sand falts that appear in purple and shades of blue which may be due to the presence of the low amount of sulfate minerals. The carbonate formations of the area exhibit red which may be due to the high reflectance of the formations. The interpretation of images shows the area of soil salinity is high (green) during the months between April and August in all the years (Fig. 5a to c) when the surface and air temperatures are high, and the humidity and rainfall are low (Govinda Rao et al., 2001). The gulf water appears in green like the similar tone of the area of gypsiferous sand and silt flats suggests that the features have nearly similar salinity during the months. Also, the images show the presence of the extent of salinity in the area of gypsiferous sand and silt flats and towards the Bay of Zekreet (dark dashed elliptical, Fig. 5), parallels to the synclinal axes and sulfate line by crossing the Rawdat Jarrah depression which may indicate the fed of gulf water from the Bay of Zekreet to the area of sabkha (Fig. 1; Dill et al., 2005; Al-Youssef, 2015; Al-Youssef et al., 2006; Ashour, 2013). On the other hand, the images of the months between September and March show the distribution of relatively low salinity in all the years (Fig. 5a to c) when compared to the months between April and August. The gulf water exhibit low salinity (blue) when compared to the area of gypsiferous sand and silt flats (green) during the months between

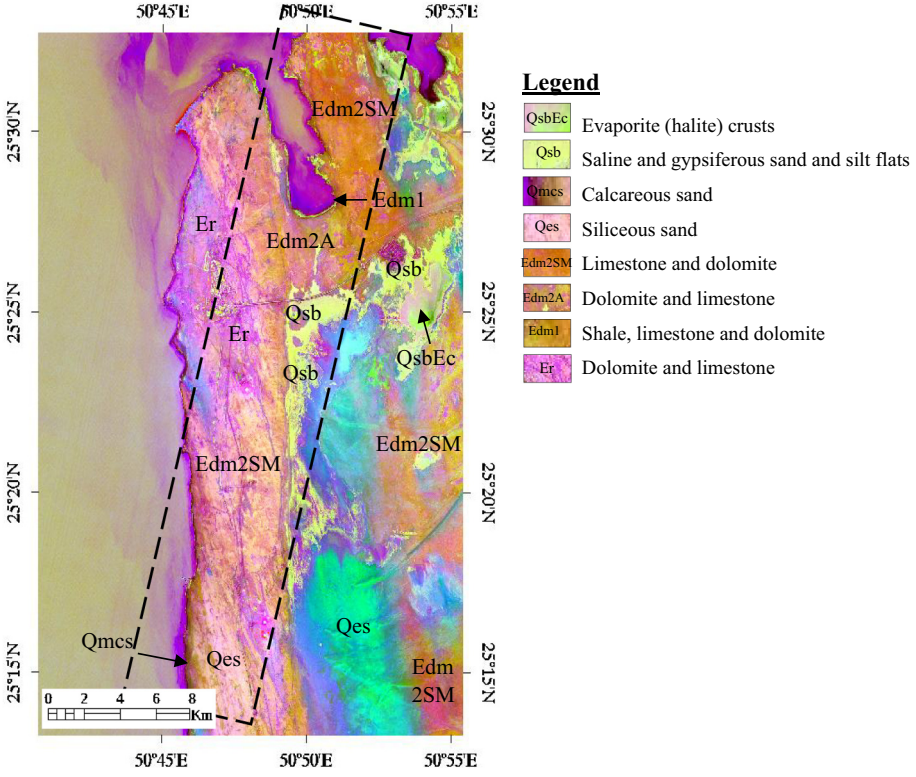

Fig. 4. ASTER principal component image (R: PC2; G: PC3; B: PC5) showing the geological formation of the Dukhan region. The dashed black rectangle represents the area of minerals mapped using Hyperion.

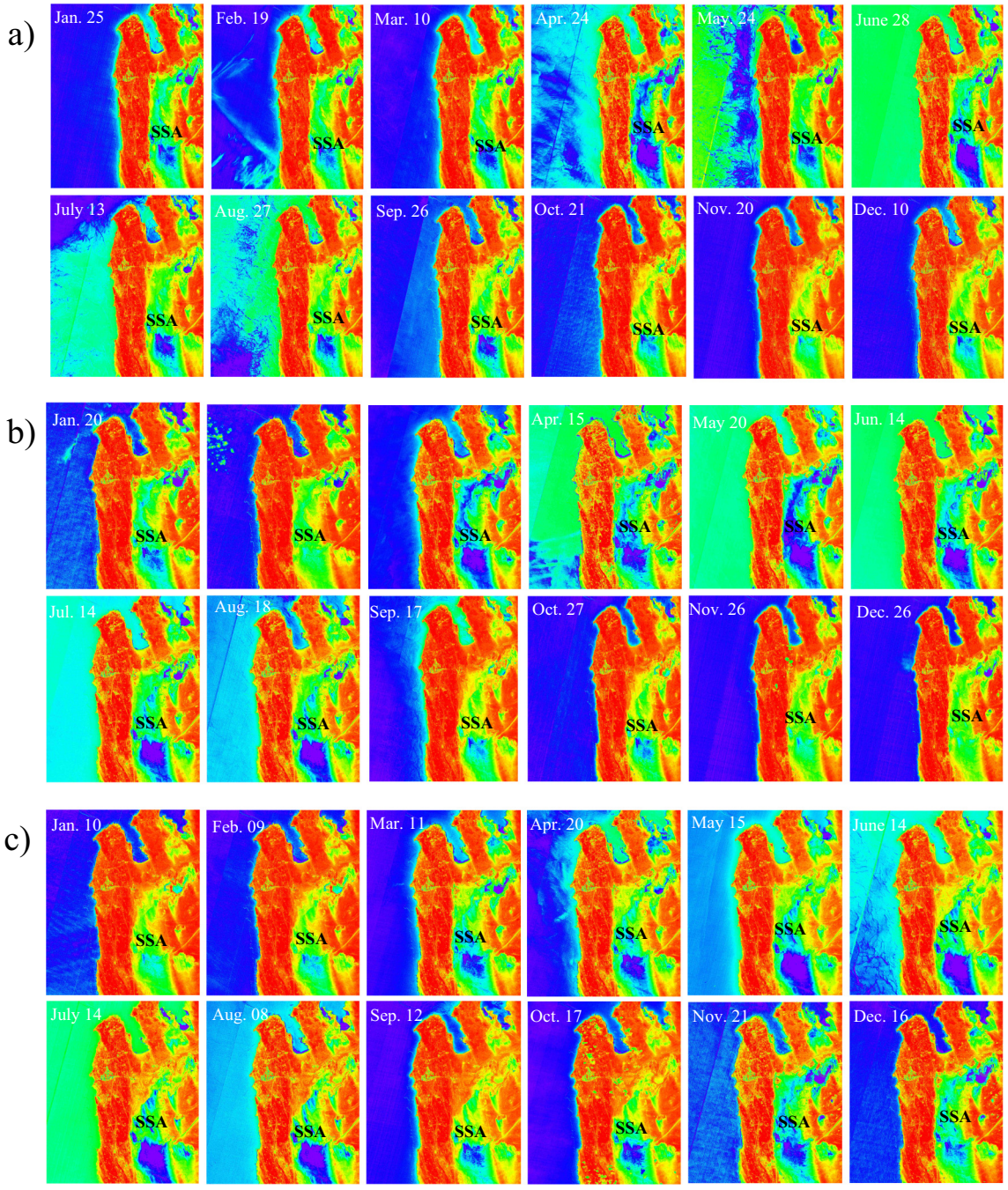

Fig. 5. Normalized Difference Salinity Index (NDSI) monthly images of MSI of the years a) 2020, b) 2019 and c) 2018 showing the area of saline soil (SSA) in green bounded by yellow in and around the area of evaporite crusts and salt flats in the Dukhan region that appear in red. (For interpretation of the references to color in this figure legend, the reader is referred to the web version of this article.)

September and March. The interpretation of the images of all months shows a gradual increase of salinity from the months of winter to the months of summer. The difference in the salinity of seawater may be due to the occurrence of low surface and air temperatures and the high humidity during the months (Al-Shaibani, 2013; Govinda Rao et al., 2001; Dhowian et al., 1987).

The high salinity of the area of gypsiferous sand and silt flats and evaporite crust were further confirmed by the study of the distribution of the types of soils of the area (Fig. 3 in Appendix-B). The study showed the occurrence of the major types of soils namely 1) the Typic Aquisalids that consist of Haplogypsids and Petrogypsids, Lithic Calcigypsids, Haplocalcids, and Lithic Haplocalcids, 2) the Typic Psammaquents and 3) the Typic Torripsamments that consist of Lithic Torriorthents in the Salids, Psamments, and Orthents Suborders within the Aridisols and Entisols Orders of soils in the study area (Hussain et al., 2010). A review of the literature shows that the Aquisalids are generally present in the areas of flat inland sabkha and or the landscape that receives saline groundwater through a lateral flow (Shomar et al., 2013; Hussain et al., 2010). The soil type is characteristic of the salinization process and is known to the presence of salt crust and salt flats that associated with water have high electrical conductivity (Hussain et al., 2010; Abdelfattah and Sahid, 2007). A comparative study of the distribution of soils (Fig. 3 in Appendix-B) with the geology (Fig. 1) showed the distribution of the Typic Aquisalids in and around the area of evaporite

crusts and salt flats in the study area. As well as, a comparative study for the distribution of Typic Aquisalids soil (Fig. 3 in Appendix-B) with the images of NDSI (Fig. 5) confirmed the spatial distribution of the salt flats and evaporite crust of the area.

4.4.2. Temporal stability of Dukhan sabkha

To understand the temporal stability of Dukhan Sabkha and to support the results of NDSI, we studied the moisture (the trace amounts of water content in liquid phase) of the sabkha area using the MSI data by the Normalized Difference Moisture index, The results are given in Fig. 6 by assigning a rainbow color (represents the lowest NDMI values in blue to the highest value by red). The images (Fig. 6) exhibit the area of moisture (MSA) in green bounded by cyan with fine texture over the area of evaporite crusts and gypsiferous sand and silt flats (Figs. 1 and 4). The evaporite crusts and the siliceous sand deposits appear in red to shades of yellow which may be due to the concentration of sulfate minerals that contain the H_2O contents. The interpretation of images shows that the moisture of the area is high over the evaporite crusts, gypsiferous sand and silt flats, and the gulf water during the months between April and August in all the years (2018 to 2020) when compared with the area of carbonate rocks which appear in purple to blue which suggest the presence of high water content in the features when compared to the carbonate formations. The images exhibit the gulf water in light green to yellow, the similar tone of the evaporite crust, and

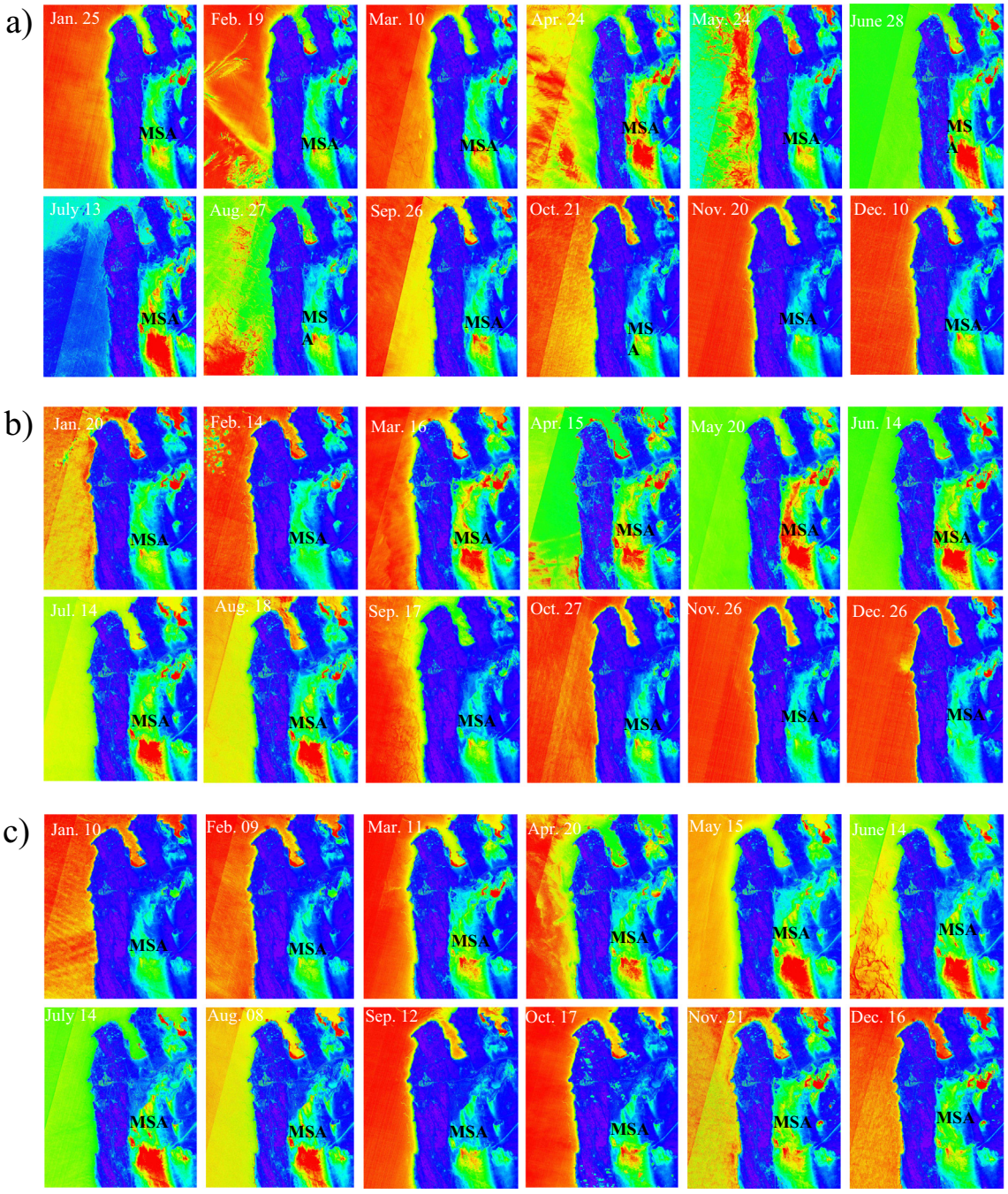

Fig. 6. Normalized difference Moisture index (NDMI) monthly images of MSI of the years a) 2020, b) 2019 and c) 2018 showing the distribution of moisture in the sabkha (MSA) in green bounded by cyan in and around the area of evaporite crusts and salt flats in the Dukhan region that appears in purple to blue. (For interpretation of the references to color in this figure legend, the reader is referred to the web version of this article.)

gypsiferous soil flats and suggest that the moisture over the features are nearly similar during the period. Whereas, the images of the months between September and March show the area of moisture is relatively low in the evaporite crusts, gypsiferous sand, and silt flats in all the years (2018 to 2020) when compared to the months between April and August. But, the moisture of the area is still high when compared to the area of carbonate rocks and suggests the presence of more moisture contents in the evaporite crust and gypsiferous soil flats. The images exhibit the gulf water in red during September and March and suggest the presence of high moisture over the gulf when compared to the moisture of sabkha. The images show the presence of the extent of moisture from the sabkha towards the Bay of Zekreet (white dashed ellipticals, Fig. 6) during summer (white ellipticals) and the occurrence may be the influence of seawater from the bay (Ashour, 2013). The interpretation of images shows clearly a gradual increase of moisture from summer to winter (Govinda Rao et al., 2001).

Thus, in this study, the utilization of 1) the hyperspectral data of Hyperion identified the major minerals of the sabkha, 2) the multispectral ASTER data discriminated the evaporites, gypsiferous sand and silt flats of sabkha, and different rock types of non-sabkha areas and 3) the MSI data showed the occurrence and extent of sabkha and the distribution of salinity and moisture of the sabkha region. The interpretations of images of the NDSI and NDMI of the years 2018 to 2020 suggest that the sabkha is not homogeneous and the distribution of salt crusts and salt flats are a dynamic and aggressive environment which is due to the changes in climatic factors, which include mainly the rainfall, temperature, moisture, and wind in the area. The results may be useful as a base to governmental decision leaders, hydrogeologists, soil scientists, construction engineers, and environmentalists to develop infrastructures and agriculture and utilize such land resources for sustainable development of the region. The application of remote sensing shed light to assess the large-time-scale environmental changes.

4.5. Field validation and laboratory studies

Fieldwork was conducted during the summer and winter of 2019 and 2020 in the study area to verify the occurrence of the minerals, rocks, soils, and saline soils of the area and to validate the results of satellite data. In the field, the occurrence of Rus and Dammam Formations (Fig. 7a, b) were verified and the presence of siliceous sand deposits over the formations are confirmed. The siliceous sand deposits of the inland have occurred with sulfate minerals (Fig. 7c). The Rus Formation occurs with dolomitic limestones and chalky limestones (Fig. 7a; Al-Saad and Hewaidy, 2020) and the Dammam formations are characteristics to mainly the limestones and fossiliferous limestones (Nummulitic limestone) (Dill et al., 2003). The occurrence of shale and marl limestone in the Dammam formation (Fig. 7d; Al-Saad, 2005) and the aeolian sand deposits over the formation (Fig. 7e) are verified in the field. The sand deposits are well-sorted and found as a non-stratified clastic windblown aeolian deposit consists of mainly feldspar, mica, and quartz grains (Nasir et al., 1999). The occurrence of sand deposits over the sabkha and sand dunes in and around the salt flats are observed. The drifting of sands, movement of the dune, and closure of roads by the sand deposits are observed in the area during June. The marine calcareous sand deposits are studied along the coast (Fig. 7f). The sabkha area is isolated in the land and the presence of gypsiferous sand and silt flats and salt crusts in the area are verified. The changes in the wetness and dryness of soils in the salt flats and crusts are studied during the summer and winter. The changes in the occurrence and extent of salt flats and crusts studied using the monthly satellite data are verified in the field. The sabkha occurs in the synclinal structure between the anticlinal structures (Figs. 1, 7g to k). The anticlinal structures are very prominent and occurred as linear ridge with the carbonate formations. The study of syncline structures and the geomorphology of the area suggests that the sabkha is intruded by seawater from the bay which is situated in the north although the Dukhan anticline relatively protects seawater intrusion besides the groundwater in the region. The occurrence of more vegetation near Dukhan and Zekreet in the northwestern part of the sabkha (Fig. 7l) and the presence of Camel race court and man-made activities in and around the salt crusts in the study area are observed.

Further, the presence of major minerals namely calcite, dolomite, gypsum, halite, anhydrite, quartz, feldspar, and mica are studied in the field (Dill et al., 2003, 2005; Nasir et al., 1999; Diloreto et al., 2019; Al-Disi et al., 2017; Brauchli et al., 2016). The study shows that gypsum, halite, and anhydrite are the most common and dominant minerals in the sabkha. The occurrence of insoluble salts and salt precipitation that developed the vast salt crust and flat due to the high rate of evaporation in the arid climate is observed (Fig. 7g to k). The gypsum is constituted in the soils of the salt flats and exhibited a dark and smooth surface (Fig. 7j, k). The concentration of more minerals along the borders of the salt crust is studied in the field. The presence of the shallow level groundwater table in the salt crust is identified by the occurrence of water in the local depressions (Fig. 7i). The salt crusts are made up of halites (Howari et al., 2002). The accumulation of halite in the local depressions after the continued evaporation due to the increase of concentrated brine in the depressions is observed. In the area of salt crust, the halites dissolve during rain and are leached into the brine and redistributed. The crystallization of halite formed a thick horizontal layer having more than 5 cm thickness (Fig. 7h). The development of salt crust in the pool during summer is studied and the salts can be removed from the topmost surface layer (Fig. 7g, h) when compared to the gypsum and calcite which are less soluble found in the gypsiferous salt flats (Fig. 7k). The crystallization of gypsum crystals at the base of the local brine pool as first and the later development of halites as a bright efflorescent in the brine pool of salt crust are studied (Fig. 7i). To confirm further the presence of minerals of the inland sabkha, the samples of minerals and rocks are analyzed by X-ray diffractogram (Fig. 4 in Appendix-B) which showed the presence of halite and gypsum in the samples collected from the salt crusts, and the gypsum, palygorskite, and kaolinite in the salt flats areas (Fig. 4a to d in Appendix-B). The analyses of limestone and dolomite samples of the Dammam and Rus Formations showed the presence of calcites in limestone and dolomites in the dolomite rocks (Fig. 4e and f in Appendix-B). Our field study suggests that the fluctuation in the water table and the evaporation processes are played a significant role in the formation and distribution of the sabkha.

Moreover, the study of soils of the salt flats showed that these are bare soils and characteristics to sandy, very loose, dense, and cemented by salts (Fig. 7j to l). The top layer consists of dry sand, silt, and salts, and has an evaporation effect (Fig. 7j, k). The soil below the layer has fine materials of plastic silt and clayey sand with organic matter which vary from place to place. The capillary action in the soils and formation of evaporite is studied in the vertical sections. It is due to the continuous evaporation at the salt flats. The measurements of salinity, Ec, TDS, and pH in the soil samples collected over the salt crust and salt flats (Figs. 1 and 3 in Appendix-B) are given in Table 1. It shows, the presence of excessively high salinity in the samples collected from salt crusts (SC) and brines (BSC) when compared to the samples of salt flats (SSF). The samples collected over the salt crusts and brine provided the maximum salinity values of 114 ppt and 116.8 ppt respectively and the very high salinity values of the brines are related to the dissolution of halite (Table 1). The salinity of the samples collected from the gypsiferous soils of salt flats provided the salinity ranges between 9.4 ppt and 46.3 ppt. The EC measured for the salt crusts and brines provided the maximum values of 175.5 mS/cm and 171.15 mS/cm respectively. The high values of EC in brine were mainly attributed to the evaporation processes and high salinity in the samples. The samples of the gypsiferous soil showed values between 25.13 mS/cm and 61 mS/cm. The measurements of TDS of the samples provided the maximum values for the salt crusts, brines, and gypsiferous soils as 141.9 g/L, 139.1 g/L, and 53.2 g/L respectively. The concentration of TDS in the samples is due to the presence

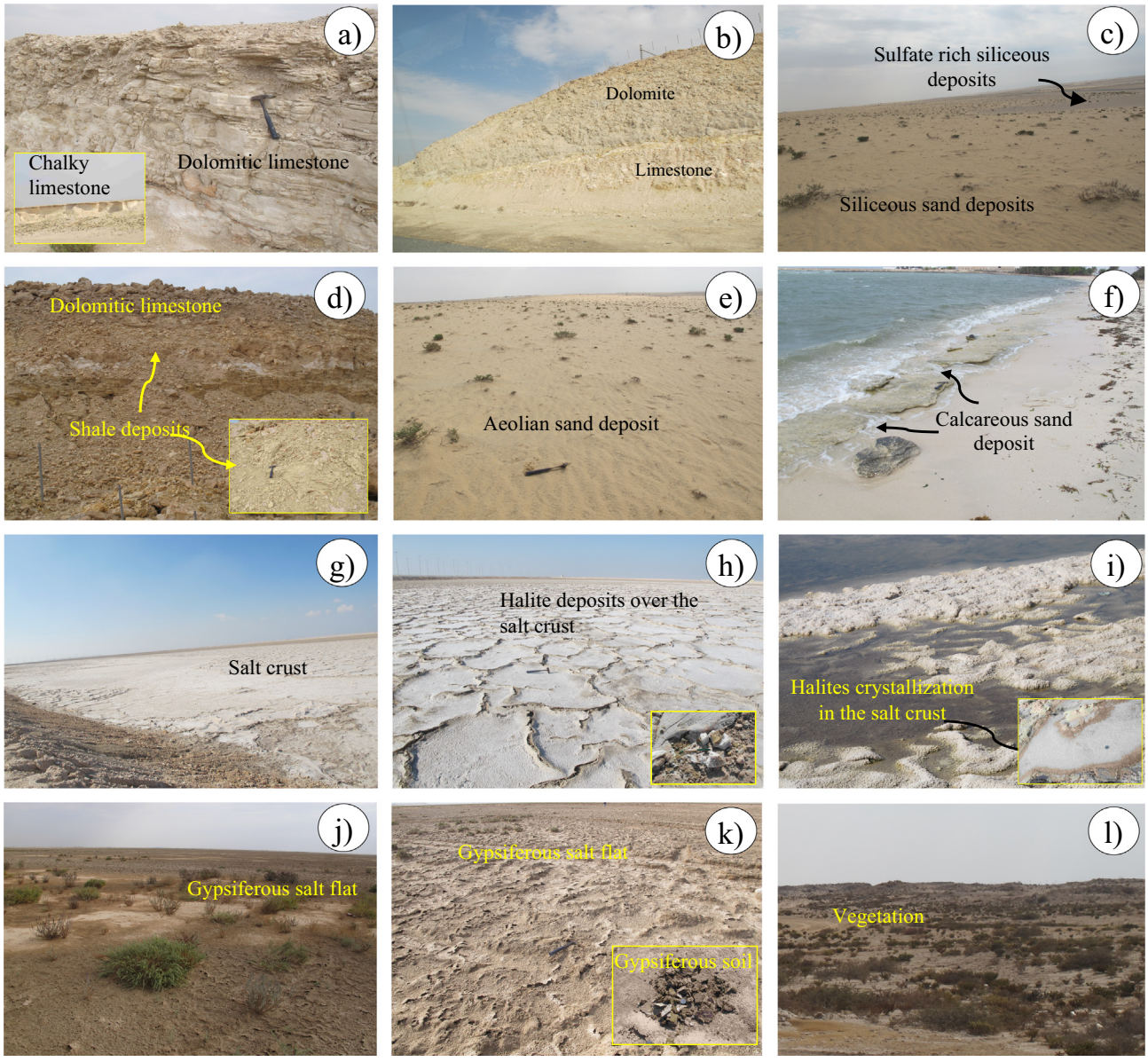

Fig. 7. Field photographs showing the occurrence of a) Rus formation, b) Dammam formation, c) siliceous sand deposit over the carbonate formation, d) shale within the Dammam formation, e) aeolian sand deposit, f) calcareous sand deposit along the coast, g) to i) salt crusts, j) and k) salt flats, and l) the vegetation distribution in the Dukhan region.

of Na^+, Ca^{2+}, Mg^{2+}, Cl^-, and $SO_4{}^{2-}$. The values of EC and TDS of the samples reflected the salinity of the area (Fig. 5 in Appendix-B). Besides, the measurement of pH for the samples of sabkha provided high values in the range between 7.15 and 8.77 (Table 1). The values measured for the samples collected over the sand and silt deposits (SSS) provided high pH and low salinity, Ec, and TDS when compared to the other samples. The study of salinity, Ec, TDS, and pH of the area confirms that the area of sabkha is under an aggressive environment due to the occurrence of saline soil and brines in and around the salt crusts and salt flats. The field and laboratory studies suggest that the sabkha poses a serious threat for any sustainable development including for the irrigation and agriculture of the area due to the irregular dehydration of gypsum.

5. Conclusions

This study utilized satellite data of Hyperion, ASTER, and MSI, and mapped the minerals, rocks, salt crusts, and gypsiferous soil flats, and studied the temporal stability of the inland sabkha that occurred near Dukhan. The interpretation of the spectral absorption features of the minerals of the salt crusts and gypsiferous soil flats showed their unique spectral absorptions in the wavelength of 1.4–1.5 μm and 1.9–2.0 μm. The minerals were detected using Hyperion data by Linear Spectral Unmixing (LSU) method and studied for their spatial distribution. The principal component image (R:PC2, G:PC3, B:PC5) developed using ASTER data showed the occurrence of the different geological formations of the area in different tones. The discrimination of formations allows us to assess the occurrence and distribution of the salt flats and crusts of the sabkha. The salinity and moisture of the sabkha region were studied using the monthly data of MSI for the years 2018 to 2020 and the distribution of salinity and moisture in the sabkha region is described. The interpretation of NDSI and NDMI images showed the variation in the occurrence and distribution of salinity and moisture which are dependent on the changes in the climate over the area. The results of remote sensing were verified and validated through field studies. The measurement of salinity, Ec, TDS, and pH parameters in

Table 1
Salinity, Ec, TDS and pH values of the brines, salt crusts, salt flats and soils of the Dukhan sabkha, Qatar.

Sample type[a]	Location	Salinity (ppt)	Electrical conductivity (mS/cm)	TDS (g/L)	pH
1 SC	25°26′1.23″N; 50°54′51.74″E	121.20	175.50	141.90	8.18
2 BSC	25°26′0.35″N; 50°54′13.52″E	116.80	171.15	139.10	8.41
3 BSC	25°25′49.31″N; 50°54′26.90″E	114.30	163.72	132.81	8.52
4 SSC	25°25′51.38″N; 50°53′46.44″E	56.90	78.20	62.70	8.39
5 SSC	25°25′52.42″N; 50°52′50.43″E	46.60	66.60	53.70	8.40
6 SC	25°25′8.90″N; 50°52′37.54″E	114.00	172.70	139.70	8.40
7 SSF	25°25′0.68″N; 50°51′52.65″E	42.70	61.00	49.50	8.47
8 SSS	25°19′30.80″N; 50°51′21.29″E	3.40	6.09	4.95	8.38
9 SSS	25°17′51.62″N; 50°51′51.64″E	4.00	7.08	5.70	8.77
10 SSS	25°17′1.24″N; 50°51′28.84″E	8.80	14.45	11.72	8.74
11 SSF	25°23′50.95″N; 50°49′28.87″E	41.90	60.00	48.70	8.28
12 SSF	25°23′5.46″N; 50°49′41.36″E	40.90	58.80	47.70	8.33
13 SSF	25°22′42.37″N; 50°50′2.84″E	27.50	41.24	33.52	8.35
14 SSF	25°22′9.32″N; 50°49′32.33″E	28.00	42.19	34.02	7.15
15 SSF	25°21′29.93″N; 50°49′32.46″E	28.90	45.37	36.64	8.25
16 SSF	25°19′42.33″N; 50°49′36.03″E	9.40	15.50	12.60	7.85
17 BSC	25°29′55.47″N; 50°54′17.27″E	109.7	149.72	113.52	8.34
18 SSS	25°28′20.11″N; 50°53′14.69″E	12.80	20.52	16.62	8.74
19 SSF	25°29′15.34″N; 50°53′46.37″E	46.30	65.50	53.20	7.96
20 SSF	25°29′35.78″N; 50°52′51.60″E	15.90	25.13	20.36	8.39

[a] SC – Salt crust; BSC - Brine in the Salt Crust; SSC – Soil in the Salt Crust; SSF – Soil of the Salt Flat; SSS – Soil over the Sand and Silt deposits.

the field samples collected from the salt crusts and salt flats suggested that the sabkha is an under-aggressive environment. This study demonstrated the potential of Hyperion, ASTER, and MSI and the capability of image processing methods to map and study the inland sabkha of an arid region.

CRediT authorship contribution statement

Sankaran Rajendran: Conceptualization, Methodology, Data Analysis and Interpretation, and Writing Original draft. Hamad Al-Saad Al-Kuwari: Investigation, Visualization and Reviewing. Fadhil N. Sadooni: Investigation, Visualization and Reviewing. Sobhi Nasir: Analysis, Editing and Reviewing. Himanshu Govil: Analysis and Reviewing.

Declaration of competing interest

The authors declare that they have no known competing financial interests or personal relationships that could have appeared to influence the work reported in this paper.

Acknowledgment

This study was supported by the Qatar National Research Fund under the National Priorities Research Program (grant no NPRP10-0214-170462). The authors are thankful to the USGS Data Management and Information Distribution (DMID) (https://glovis.usgs.gov/) for sharing the ASTER and Hyperion data, and the Copernicus, European Space Agency for sharing the Sentinel-2 data through sentinel open access hub (https://sentinel.esa.int/web/sentinel/sentinel-data-access). The measurement of spectra using the PIMA spectrometer was supported by the Sultan Qaboos University, Oman. The authors are also thankful to Mr. Dan Jerry Cortes (Gas Processing Center, QU) who carried out the XRD analysis, and Mr. Caesar Flonasca Sorino (Environmental Science Center, QU) who measured the physical parameters of field samples. Mr. Fahad Syed Asim supported the field works. The authors are thankful to Prof. Fernando A.L. Pacheco, the Associate Editor and anonymous reviewers of the journal for their valuable reviews, providing comments and suggestions that have helped to present the work lucidly. Open access funding provided by the Qatar National Library.

Appendix A. Supplementary data

Supplementary data to this article can be found online at https://doi.org/10.1016/j.scitotenv.2021.146932.

References

Abd El-Hamid, H.T., Hong, G., 2020. Hyperspectral remote sensing for extraction of soil salinization in the northern region of Ningxia. Model. Earth Syst. Environ. 6, 2487–2493.
Abdelfattah, M.A., Sahid, S.A., 2007. A comparative characterization and classification of soils in Abu Dhabi coastal area in relation to arid and semi-arid conditions using USDA and FAO soil classification systems. Arid Land Res. Manag. 21 (3), 245–271.
Abubakar, A.J., Hashim, M., Pour, A.B., 2019. Identification of hydrothermal alteration minerals associated with geothermal system using ASTER and Hyperion satellite data: a case study from Yankari Park, NE Nigeria. Geocarto International 34 (6), 597–625.
Abuelgasim, A., Ammad, R., 2019. Mapping soil salinity in arid and semi-arid regions using Landsat 8 OLI satellite data. Remote Sensing Applications: Society and Environment 13, 415–425.
Ajmal Khan, M., Böer, B., Kust, G.S., Barth, H.J., 2006. Sabkha ecosystems. West and Central Asia. vol. II. Springer, p. 179 (ISBN 978-1402050718).
Al-Amoudi, O.S.B., 1994. Chemical stabilization of sabkha soils at high moisture contents. Eng. Geol. 36 (3/4), 279–291.
Al-Amoudi, O.S.B., Abduljauwad, S.N., 1995. Strength characteristics of Sabkha Soils. Geotechnical Engineering Journal 26 (1), 733–792.
Al-Amoudi, O.S.B., Abdu1jauwad, S.N., Rasheeduzzafar, Maslehuddin, M., 1992. Effect of chloride and sulfate contamination in soils on corrosion of steel and concrete. Transp. Res. Rec. (1345), 67–73.
Al-Disi, Z.A., Jaoua, S., Bontognali, T.R.R., Attia, E.S.M., Al-Kuwari, H.A.A.S., Zouari, N., 2017. Evidence of a role for aerobic bacteria in high magnesium carbonate formation in the evaporitic environment of Dohat Faishakh Sabkha in Qatar. Front. Environ. Sci. 5 (1). https://doi.org/10.3389/fenvs.2017.00001.
Al-Hajari, S.A., Kendall, C.G.St.C., 1992. The sedimentology of the Lower Eocene Rus Formation of Qatar and neighboring regions. J. Univ. Kuwait (Sci.) 19, 153–172.
Alharbi, O.A., Phillips, M.R., Williams, A.T., Gheith, A.M., Bantan, R.A., Rasul, N.M., 2012. Desalination impacts on the coastal environment: Ash Shuqayq, Saudi Arabia. Sci. Total Environ. 421–422, 163–172.
Al-Hemoud, A., Al-Dousari, A., Al-Dashti, H., Petrov, P., Al-Saleh, A., Al-Khafaji, S., Behbehani, W., Li, J., Koutrakis, P., 2020. Sand and dust storm trajectories from Iraq Mesopotamian flood plain to Kuwait. Sci. Total Environ. 710, 136291.
Al-Homidy, A.A., Dahim, M.H., Abd El Aal, A.K., 2017. Improvement of geotechnical properties of sabkha soil utilizing cement kiln dust. J. Rock Mech. Geotech. Eng. 9 (4), 749–760.
Aljerf, L., 2016. Reduction of gas emission resulting from thermal ceramic manufacturing processes through development of industrial conditions. Scientific Journal of King Faisal University 17 (1), 1–10.
Al-Khaier, F., 2003. Soil salinity detection using satellite remote sensing. Inst. Geo-Inf. Sci. Earth Obs. 70.
Allbed, A., Kumar, L., Aldakheel, Y.Y., 2014. Assessing soil salinity using soil salinity and vegetation indices derived from IKONOS high-spatial resolution imageries: applications in a date palm dominated region. Geoderma 230–231, 1–8.

Al-Saad, H., 2005. Lithostratigraphy of the Middle Eocene Dammam Formation in Qatar, Arabian Gulf: effects of sea-level fluctuations along a tidal environment. J. Asian Earth Sci. 25, 781–789.
Al-Saad, H.A., Hewaidy, A.A., 2020. Sequence stratigraphy of the Eocene rocks in Qatar Peninsula, Arabian Gulf. Egypt. J. Geol. 64, 1–24.
Al-Shaibani, A., 2013. Economic potential of brines of Sabkha Jayb Uwayyid, Eastern Saudi Arabia. Arab. J. Geosci. 6, 2607–2618.
Al-Thani, F.A.R.H., 1992. The spatial impact of the hydrocarbon industry on land and sea use in Qatar. (Durham theses). Durham University Available at Durham E-Theses Online: http://etheses.dur.ac.uk/1626/.
Al-Youssef, M., 2015. Gypsum crystals formation and habits, Dukhan Sabkha, Qatar. J. Earth Sci. Clim. Change 6 (10), 1000321.
Al-Youssef, M., Stow, D.A.V., West, I.M., 2006. Salt Lake Area, Northeastern part of Dukhan Sabkha, Qatar. In: Khan, M. Ajmal, et al. (Eds.), Sabkha Ecosystems. West and Central Asia vol. II. Springer, pp. 163–181.
Anderson, G.P., Felde, G.W., Hoke, M.L., Ratkowski, A.J., Cooley, T.W., Chetwynd, J.H., Gardner, J., Adler-Golden, S.M., Matthew, M.W., Berk, A., 2002. MODTRAN4-based atmospheric correction algorithm: FLAASH (Fast Line-of-sight atmospheric analysis of spectral hypercubes). Proceedings Volume 4725, Algorithms and Technologies for Multispectral, Hyperspectral, and Ultraspectral Imagery VIII https://doi.org/10.1117/12.478737.
Ashour, M.M., 2013. Sabkhas in Qatar Peninsula. Landscape and Geodiversity 1, 10–35.
Bai, J., Chen, X., Li, J., Yang, L., Fang, H., 2011. Changes in the area of inland lakes in arid regions of central Asia during the past 30 years. Environ. Monit. Assess. 178, 247–256.
Bannari, A., Al-Ali, Z.M., 2020. Assessing climate change impact on soil salinity dynamics between 1987–2017 in arid landscape using Landsat TM, ETM+ and OLI data. Remote Sens. 12, 2794.
Bannari, A., Guedon, A.M., El-Ghmari, A., 2016. Mapping slight and moderate saline soils in irrigated agricultural land using advanced land imager sensor (EO-1) data and semi-empirical models. Commun. Soil Sci. Plant Anal. 47, 1883–1906.
Bannari, A., El-Battay, A., Bannari, R., Rhinane, H., 2018. Sentinel-MSI VNIR and SWIR bands sensitivity analysis for soil salinity discrimination in an arid landscape. Remote Sens. 10, 855.
Basyoni, M.H., Aref, M.A., 2016. Composition and origin of the sabkha brines, and their environmental impact on infrastructure in Jizan area, Red Sea Coast, Saudi Arabia. Environ. Earth Sci. 75, 105.
Bishop, J.L., Lane, M.D., Dyar, M.D., King, S.J., Brown, A.J., Swayze, G.A., 2014. Spectral properties of Ca-sulfates: gypsum, bassanite, and anhydrite. Am. Mineral. 99 (10), 105–2115.
Boukhary, M., Hewaidy, A.G., Luterbacher, H., Bassiouni, M.E., Al-Hitmi, H., 2011. Foraminifera and ostracods of early Eocene Umm er Radhuma Formation, Dukhan oil field, Qatar. Micropaleontology 57, 37–60.
Brauchli, M., McKenzie, J.A., Strohmenger, C.J., Fadhil, S., Vasconcelos, C., Bontognali, T.R.R., 2016. The importance of microbial mats for dolomite formation in the Dohat Faishakh sabkha, Qatar. Carbonates Evaporites 31, 339–345.
Cavalier, C., 1975. Le Tertiaire du Qatar en affleurement. Lexique Strat. Int. 3, 89–120.
Cavelier, C., Salatt, A., Heuze, Y., 1970. Geological Description of the Qatar Peninsula (Arabian Gulf): Explanation of the 1/100.000 Geological Map of Qatar. Bureau de Recherches Géologiques et Minières.
Censi, P., Sirota, I., Zuddas, P., Lensky, N., Merli, M., Saiano, F., Piazzese, D., Sposito, F., Venturelli, M., 2020. Trace element fractionation through halite crystallisation: geochemicalmechanisms and environmental implications. Sci. Total Environ. 723, 137926.
Chenchouni, H., 2017. Edaphic factors controlling the distribution of inland halophytes in an ephemeral salt lake "Sabkha ecosystem" at North African semi-arid lands. Sci. Total Environ. 575, 660–671.
Cheng, W.L., Saleem, A., Sadr, R., 2017. Recent warming trend in the coastal region of Qatar. Theor. Appl. Climatol. 128, 193–205.
Clark, R.N., 1999. Spectroscopy of rocks and minerals and principles of spectroscopy. In: Rencz, A.N. (Ed.), Remote Sensing for the Earth Sciences: Manual of Remote Sensing, third ed. vol. 3. John Wiley & Sons, New York, pp. 3–58.
Clark, R.N., King, T.V.V., Klejwa, M., Swayze, G., Vergo, N., 1990. High spectral resolution reflectance spectroscopy of minerals. J. Geophys. Res. 95, 12653–12680.
Clevers, J.G.P.W., Gitelson, A.A., 2013. Remote estimation of crop and grass chlorophyll and nitrogen content using red-edge bands on Sentinel-2 and -3. Int. J. Appl. Earth Obs. Geoinf. 23, 344–351.
Cloutis, E.A., Hawthorne, F.C., Mertzman, S.A., Krenn, K., Craig, M.A., Marcino, D., Methot, M., Strong, J., Mustard, J.F., Blaney, D.L., Bell, J.F., Vilas, F., 2006. Detection and discrimination of sulfate minerals using reflectance spectroscopy. Icarus 184, 121–157.
Crowley, J.K., 1991. Visible and near-infrared (0.4–2.5 μm) reflectance spectra of Playa evaporite minerals. Journal of Geophysical Research: Solid Earth 96, 16231–16240.
Dematte, J.A.M., Campos, R.C., Alves, M.C., Fiorio, P.R., Nanni, M.R., 2004. Visible-NIR reflectance: a new approach on soil evaluation. Geoderma 121 (1–2), 95–112.
Dhowian, A.W., Erol, A.O., Sultan, S., 1987. Settlement prediction in complex sabkha soil profiles. B. Eng. Geol. Environ. 36, 11–27.
Dill, H.G., Nasir, S., Al-Saad, H., 2003. Lithology and structural evolution of the northern sector of the Dukhan Anticline, Qatar, during the early Tertiary: with special reference to sequence stratigraphic bounding surfaces. GeoArabia 8, 201–226.
Dill, H.G., Botz, R., Berner, Z., Stüben, D., Nasir, S., Al-Saad, H., 2005. Sedimentary facies, mineralogy, and geochemistry of the sulphate-bearing Miocene Dam Formation in Qatar. Sediment. Geol. 174, 63–96.
Diloreto, Z.A., Bontognali, T.R.R., Al Disi, Z.A., Al-Kuwari, H.A., Williford, K.H., Strohmenger, C.J., Sadooni, F., Palermo, C., Rivers, J.M., McKenzie, J.A., Tuite, M., Dittrich, M., 2019. Microbial community composition and dolomite formation in the hypersaline microbial mats of the Khor Al-Adaid sabkhas, Qatar. Extremophiles 23, 201–218.
Drake, N.A., 1995. Reflectance spectra of evaporite minerals (400–2500 nm): applications for remote sensing. Int. J. Remote Sens. 16 (14), 2555–2571.
El-Battay, A., Bannari, A., Hameid, N.A., Abahussain, A.A., 2017. Comparative study among different semi-empirical models for soil salinity prediction in an arid environment using OLI Landsat-8 data. Adv. Remote Sens. 6, 23–39.
Elhag, M., 2016. Evaluation of different soil salinity mapping using remote sensing techniques in arid ecosystems, Saudi Arabia. J. Sens. 1–8 Article ID 7596175.
El-Janati, M., Soulaimani, A., Admou, H., Youbi, N., Hafid, A., Hefferan, K.P., 2014. Application of ASTER remote sensing data to geological mapping of basement domains in arid regions: a case study from the central Anti-Atlas, Iguerda inlier, Morocco. Arab. J. Geosci. 7, 2407–2422.
Elnaggar, A.A., Noller, J.S., 2009. Application of remote-sensing data and decision-tree analysis to mapping salt-affected soils over large areas. Remote Sens. 2 (1), 151–165.
ESA (European Space Agency), 2015. Sentinel -2 User Handbook. (64 pp.). https://sentinel.esa.int/documents/247904/685211/Sentinel-2_User_Handbook.
Farifteh, J., Van der Meer, F., Van der Meijde, M., Atzberger, C., 2008. Spectral characteristics of salt-affected soils: a laboratory experiment. Geoderma 145, 196–206.
Fujisada, H., 1995. Design and performance of ASTER instrument. Proc. SPIE-Int. Soc. Opt. Eng. 2583, 16–25.
Gaffey, S.J., 1987. Spectral reflectance of carbonate minerals in the visible and near-infrared (0.35–2.55 microns): anhydrous carbonate minerals. J. Geophys. Res. 92 (B2), 1429–1440.
Ge, W., Cheng, Q., Jing, L., Armenakis, C., Ding, H., 2018. Lithological discrimination using ASTER and Sentinel-2A in the Shibanjing ophiolite complex of Beishan orogenic in Inner Mongolia, China. Adv. Space Res. 62 (7), 1702–1716.
Geological map of Qatar, 2007. Center for Geographic Information Systems (CGIS), Ministry of Municipality and Environment (MME), Doha, Qatar.
Goodenough, D.G., Dyk, A., Niemann, K.O., Pearlman, J.S., Chen, H., Han, T., Murdoch, M., West, C., 2003. Processing Hyperion and Ali for forest classification. IEEE Trans. Geosci. Remote Sens. 41, 1321–1331.
Gorji, T., Yıldırım, A., Sertel, E., Tanık, A., 2019. Remote sensing approaches and mapping methods for monitoring soil salinity under different climate regimes. Int. J. Environ. Geoinf. 6, 33–49.
Govil, H., Gill, N., Rajendran, S., Santosh, M., Kumar, S., 2018. Identification of new base metal mineralization in Kumaon Himalaya, India, using hyperspectral remote sensing. Ore Geol. Rev. 92, 271–283.
Govinda Rao, P., Al-Sulaiti, M., Al-Mulla, A.H., 2001. Winter shamals in Qatar, Arabian Gulf. Weather 56, 444–451.
Guo, B., Han, B., Yang, F., Fan, Y., Jiang, L., Chen, S., Yang, W., Gong, R., Liang, T., 2019. Salinization information extraction model based on VI–SI feature space combinations in the Yellow River Delta based on Landsat 8 OLI image. Geomatics, Natural Hazards and Risk 10 (1), 1863–1878.
Howari, F.M., Goodell, P.C., Miyamoto, S., 2002. Spectral properties of salt crusts formed on saline soils. J. Environ. Qual. 31 (5), 1453–1461.
Howell, G.M., Fadhil, S., Petr, V., Jan, J., 2010. Raman spectroscopy of the Dukhan sabkha: identification of geological and biogeological molecules in an extreme environment. Phil. Trans. R. Soc. A 3683099–3683107.
Hussain, N., Abdul Rehman Alghanim, G., Ahmed, M., Ahmad El-Sharief, O., Waheed, R., 2010. Salinity management in Oman and in the region. Proceedings of the International Conference on Soils and Groundwater Salinization in Arid Countries, pp. 37–49.
Khalil, C.A., Prince, V.L., Prince, R.C., Greer, C.W., Lee, K., Zhang, B., Boufadel, M.C., 2020. Occurrence and biodegradation of hydrocarbons at high salinities. Sci. Total Environ. 143165.
Khawfany, A.A., Aref, M.A., Matsah, M.I., Taj, R.J., 2017. Utilizing Landsat-8 data in mapping of sabkha, mangroves, and land covers in Jizan coastal plain, southwestern Saudi Arabia. Arab. J. Geosci. 10 (103), 1–18.
Kumar, C., Shetty, A., Raval, S., Sharma, R., Champati Ray, P.K., 2015. Lithological discrimination and mapping using ASTER SWIR data in the Udaipur area of Rajasthan, India. Procedia Earth and Planetary Science 11, 180–188.
Leblanc, J., 2008. A Fossil Hunting Guide to the Tertiary Formations of Qatar, Middle East. p. 25 (Retrieved 19 November 2020).
Leblanc, J., 2015. A Historical Account of the Stratigraphy of Qatar, Middle-East (1816 to 2015). p. 1220 (Retrieved 19 November 2020).
Lokier, S.W., 2013. Coastal sabkha preservation in the Arabian Gulf. Geoheritage 5, 11–22.
Louis, J., Debaecker, V., Pflug, B., Main-Knorn, M., Bieniarz, J., Müller-Wilm, U., Cadau, E., Gascon, F., 2016. SENTINEL-2 SEN2COR: L2A Processor for Users. https://elib.dlr.de/107381/1/LPS2016_sm10_3louis.pdf.
Mars, J.C., Rowan, L.C., 2010. Spectral assessment of new ASTER SWIR surface reflectance data products for spectroscopic mapping of rocks and minerals. Remote Sens. Environ. 114, 2011–2025.
Metternicht, G.I., Fermont, A., 1998. Estimating erosion surface features by linear mixture modeling. Remote Sens. Environ. 64, 254–265.
Milewski, R., Chabrillat, S., Behling, R., 2017. Analyses of recent sediment surface dynamic of a Namibian Kalahari salt pan based on multitemporal landsat and hyperspectral hyperion data. Remote Sens. 9 (2), 170.
Mougenot, B., Pouget, M., Epema, G., 1994. Remote sensing of salt affected soils. Remote Sens. Rev. 7, 241–259.
Nasir, S., El-Kassas, I.A., Sadiq, A.A.M., 1999. Mineralogy and genesis of heavy minerals in coastal dune sands, South eastern Qatar. Qatar Univ. Sci. J. 19, 184–201.
Nasir, S., Al-Saad, H., Alsayigh, A., Weidlich, O., 2008. Geology and petrology of the Hormuz dolomite, Infra-Cambrian: implications for the formation of the salt-cored Halul and Shraouh islands, Offshore, State of Qatar. Jour. of Asian Earth Sciences 33, 353–365.
Nawar, S., Buddenbaum, H., Hill, J., Kozak, J., 2014. Modeling and mapping of soil salinity with reflectance spectroscopy and landsat data using two quantitative methods (PLSR and MARS). Remote Sens. 6, 10813–10834.

Nguyen, K., Liou, Y., Tran, H., Hoang, P., Nguyen, T., 2020. Soil salinity assessment by using near-infrared channel and Vegetation Soil Salinity Index derived from Landsat 8 OLI data: a case study in the Tra Vinh Province, Mekong Delta, Vietnam. Prog Earth Planet Sci 7, 1. https://doi.org/10.1186/s40645-019-0311-0.

Pearlman, J.S., Barry, P.S., Segal, C.C., Shepanski, J., Beiso, D., Carman, S.L., 2003. Hyperion, as pace-based imaging spectrometer. IEEE Trans. Geosci. Remote Sens. 41, 1160–1173.

Perkins, T., Adler-Golden, S., Matthew, M.W., Berk, A., Bernstein, L.S., Lee, J., Fox, M., 2012. Speed and accuracy improvements in FLAASH atmospheric correction of hyperspectral imagery. Opt. Eng. 51, 111707.

Rajendran, S., Nasir, S., 2015. Mapping of high pressure metamorphics in the As Sifah region, NE Oman using ASTER data. Adv. Space Res. 55 (4), 1134–1157.

Rajendran, S., Nasir, S., 2017. Characterization of ASTER spectral bands for mapping of alteration zones of Volcanogenic Massive Sulphide (VMS) deposits. Ore Geol. Rev. 88, 317–335.

Rajendran, S., Nasir, S., 2019. ASTER capability in mapping of mineral resources of arid region: a review on mapping of mineral resources of the Sultanate of Oman. Ore Geol. Rev. 108, 33–53.

Riaza, A., Buzzi, J., García-Meléndez, E., Del Moral, B., Carrère, V., Richter, R., 2017. Monitoring salt crusts on an AMD contaminated coastal wetland using hyperspectral Hyperion data (Estuary of the River Odiel, SW Spain). Int. J. Remote Sens. 38 (12), 3735–3762.

Rivers, J.M., Larson, K.P., 2018. The Cenozoic kinematics of Qatar: evidence for high-angle faulting along the Dukhan 'anticline'. Mar. Pet. Geol. 92, 953–961.

Rivers, J.M., Skeat, S.L., Yousif, R., Liu, C., Stanmore, E., Tai, P., Al-Marri, S.M., 2019. The depositional history of near-surface Qatar aquifer rocks and its impact on matrix flow and storage properties. Arab. J. Geosci. 12, 380.

Rongjiang, Y., Jingsong, Y., 2010. Quantitative evaluation of soil salinity and its spatial distribution using electromagnetic induction method. Agric. Water Manag. 97, 1961–1970.

Saeed, W., Shouakar-Stash, O., Wood, W., Parker, B., Unger, A., 2020. Groundwater and solute budget (a case study from Sabkha Matti, Saudi Arabia). Hydrology 7, 94.

Schulz, S., Horovitz, M., Rausch, R., Michelsen, N., Mallast, U., Köhne, M., Siebert, C.H., Schüth, C., Al-Saud, M., Merz, R., 2015. Groundwater evaporation from salt pans: examples from the eastern Arabian Peninsula. J. Hydrol. 531, 792–801.

Shomar, B., Amr, M., Al-Saad, K., Mohieldeen, Y., 2013. Natural and depleted uranium in the topsoil of Qatar: is it something to worry about? Appl. Geochem. 37, 203–211.

Singh, K.D., 2018. Automated spectral mapping and subpixel classification in the part of Thar Desert using EO-1 satellite hyperion data. IEEE Geosci. Remote Sens. Lett. 15 (9), 1437–1440.

Singh, M., Rajesh, V.J., Kannan, B., Bhattacharya, S., 2018. Spectral and chemical characterization of gypsum-phyllosilicate association in Tiruchirapalli, South India, and its implications. Geol. J. 53, 1685–1697.

Taghadosi, M.M., Hasanlou, M., Eftekhari, K., 2019. Retrieval of soil salinity from Sentinel-2 multispectral imagery. European Journal of Remote sensing 52 (1), 138–154.

Van der Meer, F., 1995. Spectral reflectance of carbonate mineral mixtures and bidirectional reflectance theory: quantitative analysis techniques for application in remote sensing. Remote Sens. Rev. 13, 67–94.

Wang, J., Ding, J., Yu, D., Ma, X., Zhang, Z., Ge, X., Teng, D., Li, X., Linag, J., Lizaga, I., Chen, X., Yuan, L., Guo, Y., 2019. Capability of Sentinel-2 MSI data for monitoring and mapping of soil salinity in dry and wet seasons in the Ebinur Lake region, Xinjiang, China. Geoderma 353, 172–187.

Warren, J.K., 2006. Interpreting evaporite texture. Evaporites: Sediments, Resources and Hydrocarbons. Springer, Berlin, Heidelberg, pp. 1–57 https://doi.org/10.1007/3-540-32344-9_1.

Zhang, X., Shang, K., Cen, Y., Shuai, T., Sun, Y., 2014. Estimating ecological indicators of karst rocky desertification by linear spectral unmixing method. Int. J. Appl. Earth Obs. Geoinf. 31, 86–94.